International Journal of Heat and Mass Transfer 52 (2009) 2196–2204

Contents lists available at ScienceDirect

International Journal of Heat and Mass Transfer

journal homepage: www.elsevier.com/locate/ijhmt

# Effects of compressibility and transition to turbulence on flow through microchannels

K. Vijayalakshmi [a], K.B. Anoop [a], H.E. Patel [a], P.V. Harikrishna [b], T. Sundararajan [a], Sarit K. Das [a,*]

[a] Department of Mechanical Engineering, Indian Institute of Technology-Madras, Heat Transfer and Thermal Power Laboratory, Chennai 600 036, Tamil Nadu, India
[b] Department of Electrical Engineering, Indian Institute of Technology-Madras, Chennai 600 036, India

ARTICLE INFO

*Article history:*
Received 25 June 2007
Received in revised form 19 June 2008
Available online 27 January 2009

*Keywords:*
Microchannel
Gas flow
Liquid flow
Transition
Compressibility
Non-linearity
Developing length
Transition to turbulence

ABSTRACT

A detailed experimental study of flow through long microchannels of hydraulic diameter ranging from 60.5 to 211 μm has been carried out. The internal pressure distribution along the length of the channel has been measured to analyze the local flow behaviour. The effects of compressibility and transition to turbulence occurring in the microchannel flow were investigated in detail. In addition, the resulting flow has been analyzed numerically using a commercially available CFD code, FLUENT. It has been shown that there are no special micro-scale effects, including early transition to turbulence at least in the present range of hydraulic diameters after the significant effects of compressibility are accounted appropriately.


## 1. Introduction

Microfluidics has become a subject of interest in recent times mainly due to its applicability to cooling of electronic devices. With the evolution of silicon-based integrated circuits, circuit integration has experienced an exponential increase in capacity which ultimately has resulted in higher power dissipation. For accommodating these higher heat fluxes while still maintaining the chips at optimal operating temperatures, efficient cooling technology has became the need of the hour. One such method involves the passage of coolant through microchannels etched on the silicon chip itself, thus avoiding the contact resistance problem which is prevalent in heat spreader or heat sink attachments. Cooling of this kind finds application in microchips, laser diode arrays, lab-on chip devices, microfluidic pumps, high power resistive magnets, on board cooling of propellant motors in spacecrafts, high performance microprocessors, high energy LASERs, etc.

The concept of microchannel flow was first introduced by Tuckerman and Pease [1]. Several researchers have later analyzed the flow and heat transfer phenomena in microchannels both experimentally as well as theoretically. Wu and Little [2] conducted experiments with smooth and a rough microchannel of rectangular cross-section. They observed transition to turbulence at Reynolds number as low as 400 for nitrogen gas flow and concluded that there is an effect of roughness on early transition to turbulence. The friction factors were found to be 10–30% larger than the conventional values. Pong et al. [3] investigated the pressure drop in rectangular microchannels 5–40 μm wide, 1.2 μm deep and 3 mm long, for helium and nitrogen gas flow. It was found that the pressure drop is lower than that predicted by the continuum flow and pressure profile is non-linear in the flow direction. Arkilic et al. [4] carried out experiments with helium gas flow through a microchannel of dimensions 52.25 μm × 1.33 μm × 2400 μm. A 2D analysis using the Navier–Stokes equations with slip velocity boundary condition and a perturbation solution including compressibility effects were also presented. The 2D analytical model including tangential momentum accommodation factor was seen to be in good agreement with experimental data.

Li et al. [5] investigated the flow of nitrogen through five microtubes of diameter 80–166.6 μm. They observed that the pressure drop is non-linear for Mach numbers above 0.3 and the friction factor is higher than the conventional value in this range. Chen [6] conducted a numerical study for simulating three-dimensional steady compressible flow in long microchannels. High inlet-to-outlet pressure ratios were seen to result in non-linear pressure variation due to compressibility effects; on the other hand, slip reduces the wall friction and wall curvature of pressure distribution. The predictions were in close agreement with the analytical and experimental results of Arkilic et al. [4]. Turner et al. [7] conducted a systematic investigation of laminar Nitrogen gas flow through microchannels of $D_h$ = 5–96 μm with Re = 0.1–1000. They observed

* Corresponding author. Fax: +91 044 2257 4652.
*E-mail address:* skdas@iitm.ac.in (S.K. Das).

0017-9310/$ - see front matter © 2009 Elsevier Ltd. All rights reserved.
doi:10.1016/j.ijheatmasstransfer.2008.07.056

**Nomenclature**

| | |
|---|---|
| $a$ | velocity of sound at exit of the channel, m/s |
| $A_c$ | cross-sectional area, $m^2$ |
| $D_h$ | hydraulic diameter, m |
| $f$ | friction factor |
| $H$ | depth, m |
| $L$ | length, m |
| $M$ | local Mach number |
| $m$ | mass flow rate, kg/s |
| $p$ | local pressure, Pa |
| $\Delta P$ | pressure drop, Pa |
| $R$ | characteristic gas constant, J/kg/K |
| Re | Reynolds number |
| $T$ | average temperature between inlet and outlet, K |
| $T_o$ | ambient temperature |
| $v$ | velocity of flow, m/s |
| $W_b$ | bottom width, m |
| $W_t$ | top width, m |
| $\gamma$ | ratio of specific heats for the gas |
| $\mu$ | dynamic viscosity, N-sec/$m^2$ |
| $\rho$ | density, kg/$m^3$ |

a small increase (8%) in $f$ due to compressibility as the Ma approaches 0.35 and 50% decrease in $f$ as Kn increased to 0.15. The effect of surface roughness is negligible on friction factor for both continuum and slip flow regimes. Kohl et al. [8] conducted an experimental investigation of water and air flow in rectangular microchannels of $D_h$ = 25–100 μm with internal pressure measurement. The results coincided with the theoretical predictions after considering entry region effects in liquid flow and compressibility effects in air flow. The critical Reynolds number for transition to turbulence in case of air flow was seen to depend on the channel aspect ratio ($L/D_h$).

Jiang et al. [9] carried out experiments on laminar flow of deionized water through circular and trapezoidal microchannels of hydraulic diameter ranging from 8 to 50 μm. The friction factor for circular microtubes agreed well with the conventional theory, but the friction factor for the non-circular channels was lower than that predicted from theory and varied with hydraulic diameter and length of the channel. Peng et al. [10] investigated water flow through a rectangular groove of $D_h$ = 133–367 μm, in the Reynolds number range of 8–800. The friction factor was observed to be higher than the predicted values and it was also not inversely proportional to Re in the laminar regime. Nguyen et al. [11] observed transition to turbulent flow for Re = 1000–1500, in microchannels 500 μm deep and 1707 μm wide with trapezoidal cross-section. Richter et al. [12] conducted experiments with water in trapezoidal microchannels of maximum width ranging between 28 and 182 μm, etched on silicon wafers. They observed that the pressure drop is linearly proportional to flow rate and that it can be predicted accurately using conventional theory if the viscosity variation with temperature is considered.

Friction factor for water flow in smooth and rough microchannels of hydraulic diameters between 128 and 521 μm with high aspect ratio was investigated by Pfund et al. [13]. It was shown that for a microchannel with 3% relative roughness, the friction factor is higher than that predicted by conventional theory. Li et al. [14] measured the friction factors for de-ionized water flow in microtubes made of glass, silicon and stainless steel. They observed that for fully developed laminar flow, the Poiseuille number (product of $f$ and Re) is 64, in microtubes for glass and silicon; on the other hand, for rough microtubes made of stainless steel, the measured friction factors were higher than the predicted values. The Reynolds number corresponding to transition to turbulent flow was in between 1700 and 2000. Wu and Cheng [15] measured the friction factor for laminar flow of deionized water in silicon microchannels of trapezoidal cross-section with hydraulic diameter 25.9–291 μm. The experimental data were found to be in good agreement with the existing analytical solution for an incompressible, fully developed laminar flow with no-slip boundary condition and the transition to turbulent flow occurred at a Reynolds number of 1500–2000. Hao et al. [16] measured instantaneous velocity fields in smooth and rough rectangular microchannels with hydraulic diameter ranging from 153 to 191 μm, using micro-PIV. It was observed that for a smooth channel, transition occurs at Re = 2100 whereas for rough microchannels early transition is observed in the range Re = 900–1100. Renksizbulut and Niazmand [17] made three-dimensional numerical analysis on a trapezoidal microchannel particularly in the entrance region of flow. A new correlation was proposed for both friction factor as well as Nusselt number in the flow developing region. It was also argued that entrance length was a weak function of aspect ratio for a specified side angle and was more significant for short channels.

From the above literature review, it is clear that several experimental and theoretical studies are available for microchannel flow but many deviations have been observed from the conventional theory, mainly with respect to friction factor variation and transition from laminar to turbulent flow. Also, most of the experimental results contradict each other presumably due to the inability to distinguish between the effects due to compressibility and transition to turbulence. Very few of the above studies have considered the local behaviour of flow through the channel. Reviews by Colin et al. and others [18–20] indicate that the sources of discrepancy for the microchannel flow may lie on the effects due to compressibility and surface roughness rather than any size effect.

Hence, in the present study, it is intended to characterize the true behaviour of microchannel flow and isolate the effects of different influencing factors. The main objective is to investigate the physics of fluid flow, particularly with respect to transition to turbulence and compressibility effects for the channels in the range of 60 μm and 211 μm hydraulic diameter, with the help of pressure measurements along the length of the channel. It is also desired to test the applicability of conventional fluid mechanic models in this range of hydraulic diameter. This is done by carrying out a numerical simulation using the Navier–Stokes equations with no-slip at the channel walls and comparing the results with experimental data.

## 2. Experiments

### 2.1. Fabrication of microchannel

Microchannels were fabricated on a p-type silicon ⟨100⟩ single side polished wafer of 500 μm thick, by photolithographic and wet etching processes which were done in a class 100 environment. The silicon wafer was cleaned properly to remove metal impurities, if any, present on the surface. An oxide layer of 0.8 μm thick was grown on the silicon surface by wet oxidation method. A Positive Photo Resist (PPR) was spin coated on to the oxidized silicon surface at 4000 rpm. The channel region was exposed to UV radia-

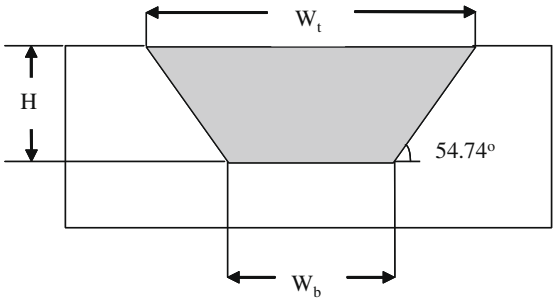


**Fig. 1.** Channel cross-section.

tion through a mask so that the exposed PPR portion gets weakened. The exposed PPR was removed by a developer and the oxide layer below that was removed by buffered hydrofluoric acid (BHF). Finally the exposed silicon surface in the channel portion was etched out by 30% KOH solution at 75 °C. The resulting channel depth depends on the time of etching process whereas the channel roughness depends on the concentration of KOH solution. The channel cross-section is shown in Fig. 1.

Microchannel of nominal length of 52 mm was etched on silicon wafers. Two ports of $4 \times 4$ mm dimensions were made at either end, with a centre to centre distance of 56 mm, which facilitated the entrance and exit of the flow through the channel. Three such channels were made with different hydraulic diameters, keeping the aspect ratio almost the same ($H/W_t \approx 0.3$), whose dimensions are given in Table 1. For pressure measurement, tappings were made on a thick acrylic sheet by drilling holes of 2 mm diameter at different positions aligned along the length of the channel. Five such equidistant tappings with 14 mm gap were taken along the length of the channel including at inlet and exit ports. The top view of acrylic sheet aligned with the channel is given in Fig. 2. Another plate with a thick cushioning pad was used to support the channel from the bottom. Thus the microchannel was sandwiched between two plates and tightly clamped mechanically. Two side holes were also drilled in between each tapping on either side, on the top acrylic sheet. No leak through the side holes ensured that the flow was only through the channel without side spreading and contact between the wafer and the top plate was also ensured to be perfect. Also for the flow analysis Knudsen number was calculated and was found to be of the order of $10^{-4}$ which ensures a continuum flow regime without slip or rarefaction effects. The above fact can be seen clearly from Fig. 3, which shows the variation of Mach number with Reynolds number for two channels with hydraulic diameter 60 μm and 211 μm.

### 2.2. Experimental setup

In gas experiments, nitrogen was used as the working fluid. The basic experimental setup consists of a nitrogen gas cylinder (at 120 bar) fitted with a pressure regulator (0–16 bar) providing controlled pressure at inlet, a particle filter (5 μm) and a flow control valve as shown in Fig. 4. The cylinder pressure was reduced at the test section inlet by the pressure regulator. The inlet ($T_1$) and exit ($T_2$) temperatures were measured with K type thermocouples with an accuracy of 0.1 °C. Pressure measurements were done with a pressure transducer having a range of 0–10 bar. The flow rate of the gas was measured using the volume displacement technique. The flow from the exit of the channel was directed to an inverted measuring jar filled with water, so that gas displaces water in the jar. The time taken to displace a particular volume of water was measured, from which directly the volume flow rate of the gas flow was calculated. Uncertainty analysis is carried out to esti-

**Table 1**
Channel dimensions.

| S. No. | Top width, $W_t$ (μm) | Depth, $H$ (μm) | Hydraulic diameter, $D_h$ (μm) | Cross-sectional area ($m^2$) | Surface roughness, Ra (nm) |
|---|---|---|---|---|---|
| 1 | 540 | 150 | 211 | $6.51 \times 10^{-8}$ | 75.05 |
| 2 | 300 | 91.5 | 124 | $2.15 \times 10^{-8}$ | 86.16 |
| 3 | 130 | 50 | 60.5 | $4.72 \times 10^{-9}$ | 109.88 |

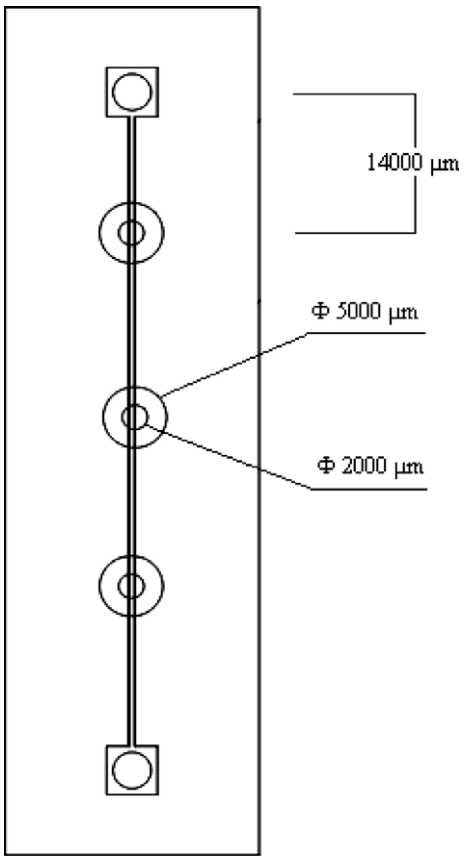


**Fig. 2.** Top view of channel with top acrylic sheet.

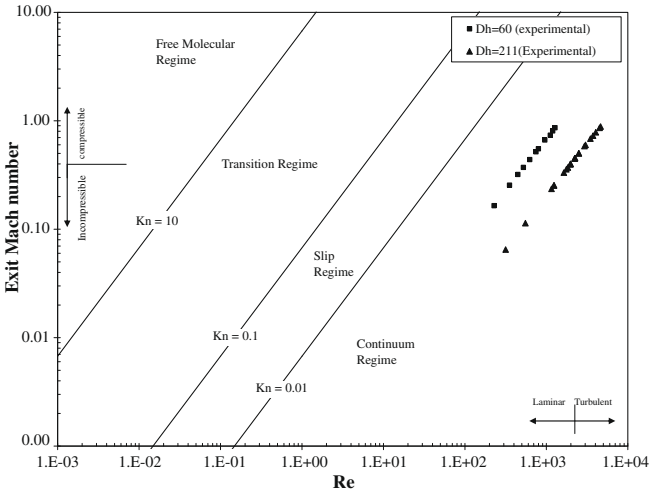


**Fig. 3.** Variation of exit Mach number with Re.

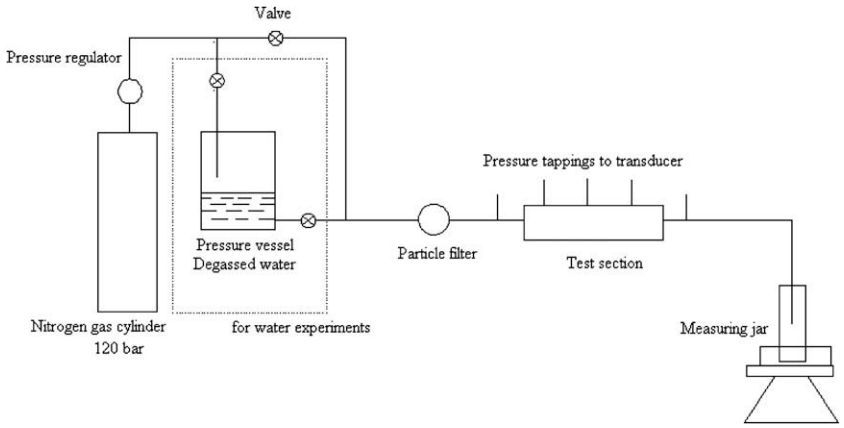


**Fig. 4.** Schematic diagram of experimental set up for gas/water flow.

**Table 2**
Uncertainties in the experiment.

| | $D_h$ = 211 μm (%) | $D_h$ = 124 μm (%) | $D_h$ = 60.5 μm (%) |
|---|---|---|---|
| Hydraulic diameter, $D_h$ | 0.86 | 0.08 | 5.95 |
| Area, $A_c$ | 3.13 | 0.10 | 0.15 |
| Re | 8.70 | 4.46 | 19.19 |
| $f$ | 5.34 | 0.12 | 4.14 |

mate the errors in both measured values and derived quantities. Using standard procedure, the uncertainties involved in channel dimensions, measured data of pressure drop and flow rate and the derived parameters of Reynolds number (Re) and friction factor ($f$) were calculated and these are given in Table 2.

The set up used for water experiments, is the same as that of gas flow experiments except for the addition of a pressurizing vessel (indicated inside the dotted line, in Fig. 4). High pressure nitrogen gas, contained in a gas cylinder at 120 bar, was regulated to lower pressures by a pressure regulator of 0–15 bar range and used to pressurize the water in the vessel. Water was degasified before sending into the experimental circuit because whenever water undergoes a high pressure drop inside the channel, the dissolved gases evolve and form bubbles in the flow lines. Before starting the experiments, the entire system was flushed with water to remove gas bubbles, if any. The volume flow rate of water coming out of the channel was measured by collecting water in a measuring jar.

## 3. Numerical investigation

In order to simulate the flow through microchannels, an axi-symmetric geometry shown in Fig. 5 having the same hydraulic diameter as the microchannels investigated experimentally, was considered. The axi-symmetric geometry was chosen in order to reduce the computational effort and also due to the fact that only the axial variation of pressure (and not the local velocity profile) was possible to be measured by the experiments. Hence, the average cross-sectional pressure could be compared, with the wall static pressure computed by the axi-symmetric model with a reasonable level of accuracy. Based on many computational trials made using axi-symmetric and trapezoidal geometries, it was observed that the pressure profiles (static Pressures) for Trapezoidal and axi-symmetrical geometries, showed reasonable agreement (as shown in Fig. 6, for a Re = 1200 and $D_h$ = 211 μm) and due to the computational simplicity an axi-symmetric geometry was used in further analysis. The geometry was created in GAMBIT 2.0 and the channel domain was divided into small quadrilateral cells. The meshing was done in such a way that it is fine at channel walls and near the channel-port boundary, because in these regions sharp variations in velocity and pressure take place. The pressure inlet and pressure outlet boundary conditions were prescribed at the inlet and exit ports. The walls were assumed to be adiabatic with no-slip and symmetry boundary condition was assigned along the axis of the channel. The simulation was carried out in the commercial CFD software FLUENT 6.2. A grid independence study was carried out to examine the effect of grid size, to assure convergence of results. The result of the grid independence study is shown in Table 3. Since beyond 30 × 10,400, the reduction in exit velocity was less than 1%, this grid was used in the entire study.

In case of gas flow, the simulation was carried out by coupling the continuity and the momentum equations. The energy equation was also solved by second order upwind implicit scheme in order

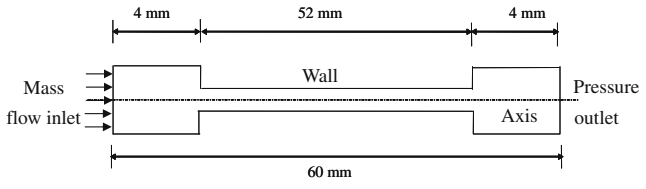


**Fig. 5.** Axi-symmetric geometry for simulation.

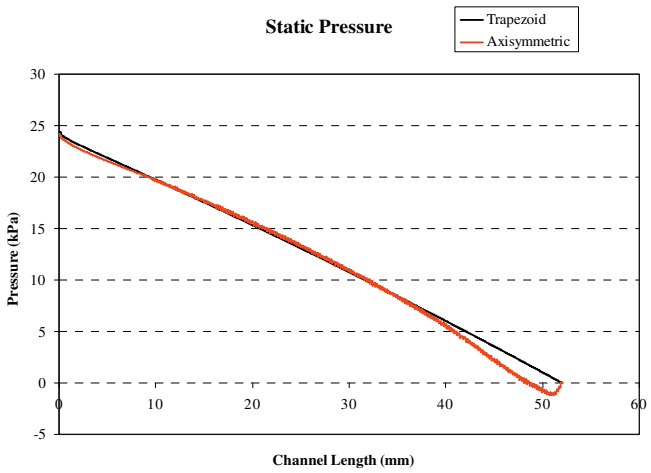


**Fig. 6.** Comparison of static pressures for trapezoidal and axi-symmetric cross-sections for $D_h$ = 211 μm.

**Table 3**
Grid independence study.

| Grid | $V_{out}$ (m/s) | % Difference |
|---|---|---|
| 30 × 6500 | 62.68 | – |
| 30 × 10,400 | 59.05 | 5.9 |
| 36 × 13,000 | 58.72 | 0.55 |

to take care of the viscous dissipation effects. The pressure–velocity coupling was ensured by the SIMPLE algorithm. Nitrogen gas was modelled as an ideal gas. The other properties like viscosity, thermal conductivity and specific heat at constant pressure, were assumed to be constants. The water flow was simulated by considering the conservation equations for mass and momentum. The flow was modelled by keeping density and viscosity as constants. In both situations of gas and water flows, the value of critical Reynolds number where the transition from laminar to turbulent flow takes place was taken from the experimental observations and the flow was modelled by giving laminar conditions for Re below the critical Reynolds number, and beyond this Re, the simulation was carried out using the standard $k$–$\varepsilon$ model.

## 4. Results and discussion

### 4.1. Experimental results

Experiments were conducted with three microchannels of different hydraulic diameters but with almost similar aspect ratio of $H/W_t \approx 0.3$ and surface roughness, so that the effect of size on the flow behaviour can be investigated. The pressure distribution for the gas flow through a channel with $D_h = 211$ μm, plotted along the length of the channel, is shown in Figs. 7 and 8. It is clearly seen from Fig. 7 that for Reynolds numbers up to 1600, the pressure distribution is linear as expected in incompressible flow. For Re beyond 1600, the pressure distribution shows some non-linearity near the exit, indicating the compressible nature of flow. The slight non-linearity of pressure profile near the entry in Fig. 7 for the higher Re cases, is likely to be due to entrance length effects because compressibility effects come into picture near the exit region only. Further for gas flow through a channel of $D_h = 211$ μm, the exit Mach number approaches 0.3 at Re ≈ 1600, which illustrates that the non-linearity in pressure profiles in Fig. 8 is due to compressibility effects. In fact, the pressure gradient towards exit of the channel is very high in compressible flow regime because of the flow acceleration. For water flowing through the same channel, the pressure distributions for the whole range of Reynolds number are linear as the flow is incompressible, as shown in Fig. 9. In the higher Re cases, slight non-linearity is seen near the inlet of the channel indicating typical behaviour of a developing flow. Further, the pressure distributions of both gas and water flow confirm the fact that the occurrence of non-linearity in the later part of the channel for gas flow, is due to compressibility. This is evident from the trend that at the same Reynolds number, the pressure distribution is linear near the exit, in case of water flow.

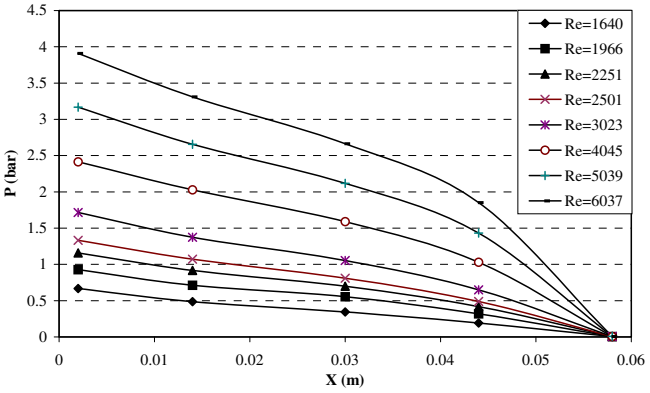


**Fig. 8.** Pressure distribution for gas flow through $D_h = 211$ μm at higher Re.

In order to represent the pressure drop in a non-dimensional form, the friction factor was calculated by using three different equations, as given below:

From Darcy equation for incompressible flow,

$$f = \frac{2\Delta p D_h}{\rho L V^2} \tag{1}$$

where, the total pressure drop between inlet and exit parts is given by,

$$\Delta p = (p_{in} - p_{out}) - \frac{\rho v^2}{2}(K_c + K_e + K_{dev})$$

In the above expression, $K_c$ and $K_e$ are the calculated contraction and expansion loss coefficients based on the area ratios (White [21]). $K_{dev}$ is the loss coefficient associated with developing length, which is given in Turns [22].

In the present analysis attempts to separate out the effects of compressibility and transition to turbulence effects is carried out by analysis of $f$Re vs Re and $f$ vs Re plot. The sudden change from laminar to turbulent flow is better observed in $f$ vs Re plot while the steady and gradual change from incompressible to compress-

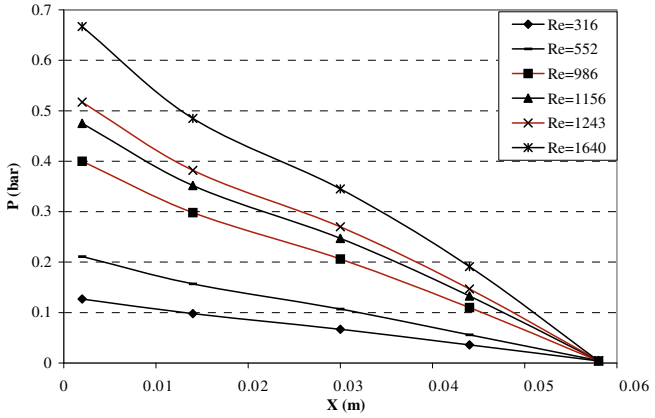


**Fig. 7.** Pressure distribution for gas flow through $D_h = 211$ μm at lower Re.

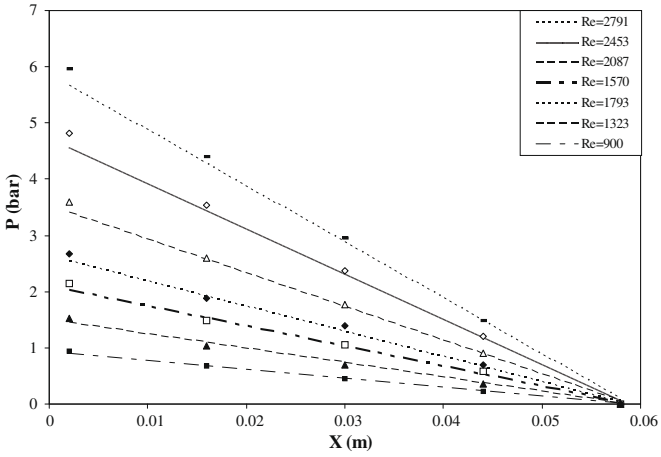


**Fig. 9.** Pressure distribution for water flow through $D_h = 211$ μm.

ible flow is better visualized in $f$Re vs Re plot. In the case of compressible flow through the channel, two equations are used to calculate the friction factor; one by assuming the flow as isothermal and the other by assuming it as adiabatic. Actually, these are the two extreme situations for a compressible flow. The actual gas flow may follow a polytropic process which lies in between the adiabatic and isothermal cases.

For isothermal compressible flow, friction factor given by White [21] is

$$f = \frac{D_h}{L}\left(\frac{1-\gamma M_1^2}{\gamma M_1^2} - \frac{1-\gamma M_2^2}{\gamma M_2^2} + \ln\frac{M_1^2}{M_2^2}\right) \tag{2}$$

For adiabatic compressible flow, Kohl et al. [8] show that

$$f = \frac{D_h}{L}\left\{\frac{P_1^2}{RT_1(\rho u^2)}\left(1-\frac{P_2^2T_1}{P_1^2T_2}\right) + \frac{\gamma+1}{2\gamma}\ln\left[\frac{T_1}{T_2}\frac{2P_2^2\gamma+(\gamma-1)\rho u^2RT_2}{2P_1^2\gamma+(\gamma-1)\rho u^2RT_1}\right]\right\} \tag{3}$$

The friction factor in turbulent flow regime is compared with the Blasius equation of the form

$$f = 0.316\mathrm{Re}^{-1/4}. \tag{4}$$

In incompressible flow through constant area ducts, the friction inside the duct affects only the pressure drop, average velocity remains constant in this case. In the incompressible fully developed flow regime, the product of friction factor and Reynolds number ($f$Re) is a constant. In compressible flows friction affects the pressure, density and hence velocity. Thus, in compressible flows, density variations must be accounted for in the calculation of friction factor. Generally, the deviation in $f$Re from laminar incompressible constant value is either due to the transition from laminar to turbulent flow or due to the onset of compressibility effects at nearly 0.3 Mach number. The transition to turbulent flow can be clearly distinguished from the compressibility effects, from $f$ vs Re graph, where the slope of the $f$ curve changes from one straight line to another due to the onset of transition to turbulence. In the present study, the friction factor, $f$ was calculated by using incompressible and compressible Eqs. (1)–(3), and compared with the Blasius Eq. (4) in the turbulent regime.

Fig. 10 shows $f$Re drawn against Re for gas and water flows through a channel of $D_h$ = 211 μm. At lower Re, both water flow and gas flow results coincide and have a constant value as expected in the case of laminar incompressible fully developed flow. This indicates that along with water, gas flow can also be treated as incompressible in this range of Reynolds numbers. The constant value of $f$Re is observed to be 53 for the trapezoidal geometry of the channel used in the present case. Also $f$Re = 53 is matching with the same calculated by Eq. (5) given by Renksizbulut and Niazmand [17]

$$(f\mathrm{Re})_{fd} = 13.9\left(\frac{90^\circ}{\phi}\right)^{-0.07} + 10.4\exp\left[-3.25\alpha\left(\frac{90^\circ}{\phi}\right)^{0.23}\right] \tag{5}$$

where $\alpha = \frac{\text{Height}}{\text{Bottom width}}$ and $\phi$ is the inclination angle for the trapezoidal geometry.

At Re ≈ 1600, the water and gas results start deviating suddenly from the constant value and both are following a similar trend parallel to the Blasius curve given by Eq. (4), indicating turbulent flow behaviour. Hence Re ≈ 1600 can be identified with the transition to turbulence. The transition Reynolds number seems to be slightly less than the usual transition value in conventional channels (Re = 2000–3500). The reason may be the presence of sharp edges at inlet in the channels used in the study. The higher value of relative roughness could also be another cause for the slightly lower transition Re value. The difference between the experimental values and the Blasius curve is due to the fact that the Blasius expression corresponds to incompressible-turbulent flow through circular ducts, whereas in the present case, compressible turbulent flow occurs in trapezoidal microchannels. Further a slight deviation is observed between the adiabatic and isothermal compressible equations at higher Reynolds numbers. During the onset of compressible flow, where the velocities are less and sufficient time is available to transfer heat through the walls, the process follows a path close to the isothermal trend. For highly compressible flows, where the flow rates are very high and hence no time is available for heat transfer, the flow is close to the adiabatic case. At moderate compressible flows, the process may be polytropic and the $f$Re curve lies in between the adiabatic and isothermal curves. Transition to turbulence can be further confirmed by the curve of $f$ vs Re in Fig. 11, since the slope of the $f$ curve changes at Re ≈ 1600. Further for gas flow, exit Ma = 0.3, at Re ≈ 1600. Hence, the compressibility effects are also occurring at similar Reynolds numbers as transition to turbulence, in this particular case. For this reason, it is difficult to differentiate between the two effects for the flow through the channel of $D_h$ = 211 μm.

Both transition to turbulence and compressibility effects can be clearly distinguished for flow through a channel with smaller cross-section, of $D_h$ = 124 μm. In Fig. 12, $f$Re values of both water and gas follow a constant line at lower Reynolds numbers indicating incompressible fully developed flow behaviour. At around Re = 800–900, the gas results start deviating from the constant value of 53. The exit Ma approaches 0.3 at Re ≈ 850; hence, the change in $f$Re curve at this Reynolds number is presumed to be due to the onset of compressible flow. Beyond this range, water re-

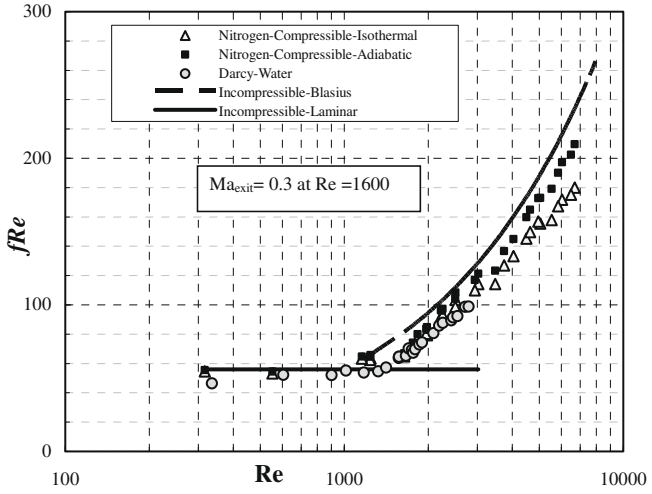


**Fig. 10.** $f$Re vs Re for $D_h$ = 211 μm.

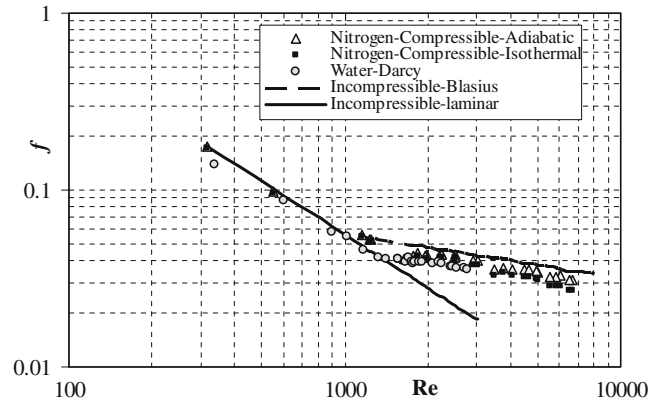


**Fig. 11.** $f$ vs Re for $D_h$ = 211 μm.

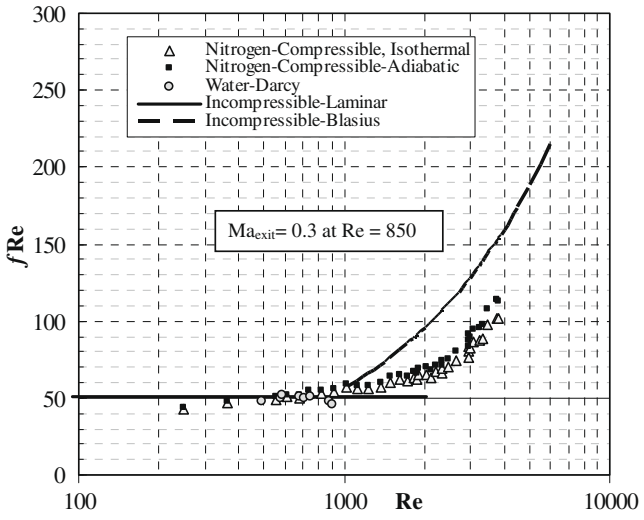


**Fig. 12.** $f$Re vs Re for $D_h$ = 124 μm.

sults continue to follow the trend of $f$Re = constant, which confirms the fact that the deviation in the case of gas flow is due to compressibility effects. It should be noted here that for gas flow above Re ≈ 850, although the $f$Re curve deviates from the constant value it is not parallel to the Blasius curve, which is another indicator that this deviation is not due to transition to turbulence. The experimental values follow a similar trend as the Blasius curve (i.e., parallel to the Blasius curve) beyond Re of around 2300, indicating transition to turbulent flow. The transition can more clearly be observed in Fig. 13, where the slope of $f$ changes in the range of Re ≈ 2100–2300. Thus, the deviation of $f$Re from laminar incompressible constant value as observed in Fig. 12, is definitely due to compressibility effects but not due to transition to turbulent flow, since there is no corresponding change in the slope of $f$ curve near Re = 850 in Fig. 13. Hence in this case, the compressibility and transition effects are well distinguished and compressible flow has started at a smaller the value than transition to turbulent flow.

For the gas flow through the channel of $D_h$ = 60.5 μm, exit Ma reaches a value of 0.3 at Re = 430. Hence, the flow becomes compressible even at this lower Reynolds number. The value of $f$Re in

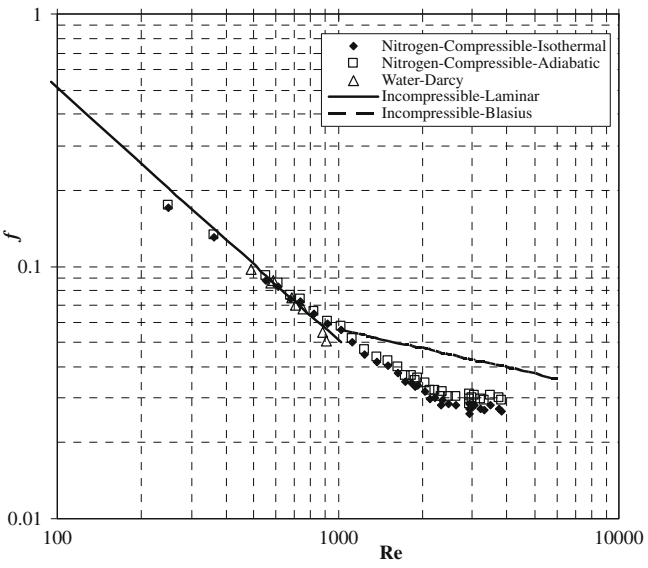


**Fig. 13.** $f$ vs Re for $D_h$ = 124 μm.

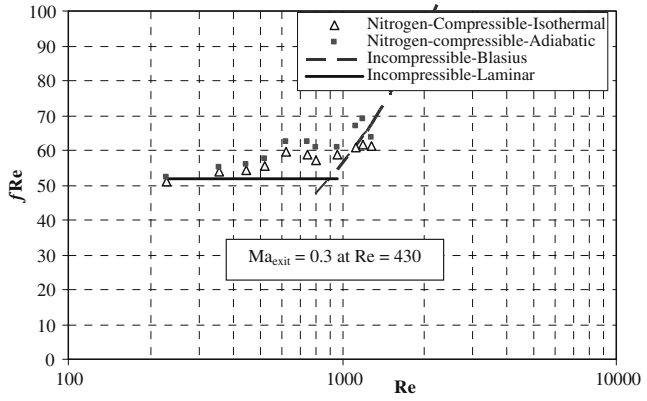


**Fig. 14.** fRe vs Re for $D_h$ = 60.5 μm.

the laminar incompressible regime is still around 53, but it starts deviating from the constant value of around a Reynolds number of 400, as shown in Figs. 14 and 15 depicts the $f$ vs Re plot which draws the same conclusions as the previous figure. In all the three cases experiments were limited to a maximum possible Reynolds beyond which pressure drops are too high to be handled by the flow circuit. On the lower side also, the limiting Re was based on the flow rate below which measurement accuracy will become poor.

## 5. Numerical results

### 5.1. Validation with experimental results

The axial pressure profiles obtained by numerical simulation are compared with the corresponding experimental results for the channels of hydraulic diameters 211 μm, 124 μm and 60.5 μm.

For gas flow through the channels, the simulated results are compared with experimental data in Fig. 16, for a few Reynolds numbers covering all the regimes of interest. It was seen in the experimental results of Fig. 10 earlier that for a channel of $D_h$ = 211 μm, the transition to turbulence as well as the effects of compressibility start at a similar Re of 1600. Hence, Fig. 16 shows the validation of numerical predictions for the flow through the channel of $D_h$ = 211μm and Re = 4525 in the turbulent-compressible regime. It also gives the validation of results for the gas flow through the channel of $D_h$ = 124 μm at Re = 1240, which corresponds to the laminar-compressible regime, since for this hydrau-

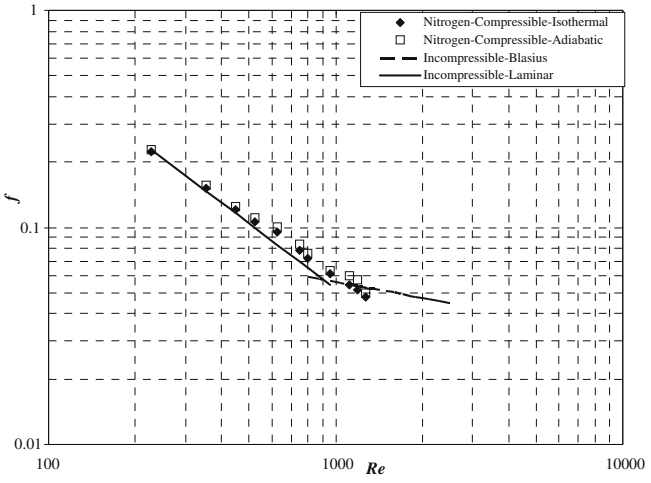


**Fig. 15.** f vs Re for $D_h$ = 60.5 μm.

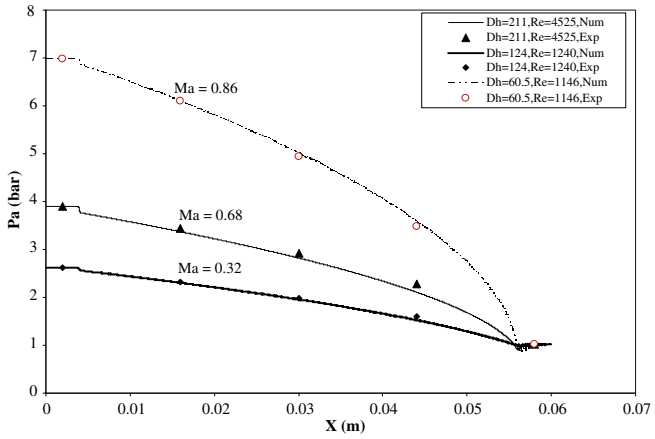


**Fig. 16.** Validation with experimental results for gas through three channels at different Re.

lic diameter, compressibility effect starts at Re = 850 (Fig. 12). Similarly, the validation in the case of $D_h$ = 60.5 μm and Re = 1146 in laminar-compressible regime, is also shown in Fig. 16, since the onset of compressibility is observed experimentally at Re = 400

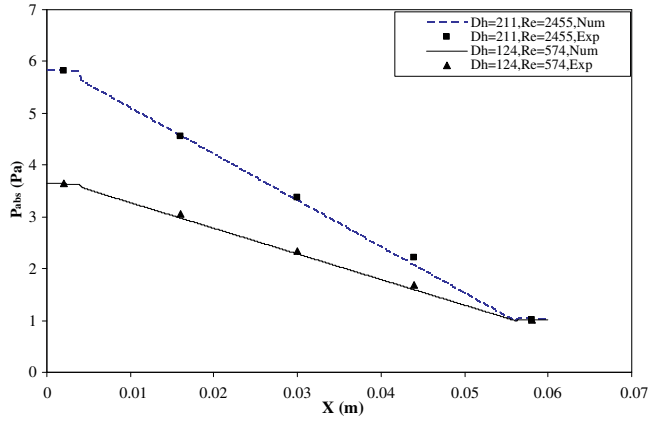


**Fig. 17.** Validation with experimental results for water through $D_h$ = 211 μm at Re = 2455 and through $D_h$ = 124 μm at Re = 574.

(Fig. 14). The pressure profiles show a constant value in the inlet and exit port regions, where the pressure is almost same at all points. Further, we can observe a dip in the pressure at the channel inlet, which is due to the contraction loss between the port and the channel. The pressure reduces continuously from the inlet to the exit of the channel in a non-linear fashion, which indicates the compressible nature of flow within the channel for the cases considered. In the later part of the channel non-linear pressure variation is prominent; hence the effect is mainly due to compressibility but not due to boundary layer development. At the channel exit, a small rise is observed, associated with the pressure recovery caused by expansion in the flow area from the channel to port. However, this pressure recovery does not commensurate with the Mach number at the exit, because of expansion losses.

In the case of water flow, the predicted results are compared with the experimental pressure values in Fig. 17 for flow through channels of $D_h$ = 211 μm (at Re = 2455) and $D_h$ = 124 μm (at Re = 574) corresponding to turbulent and laminar flows, respectively. Here the pressure profiles are found to be almost linear within the channel due to the incompressible nature of flow. In all the cases described above, it is observed that the simulation is in very good agreement with the experimental results for local pressure along the channel over a wide range of Reynolds numbers covering different regimes (laminar incompressible, laminar compressible, turbulent incompressible and turbulent compressible). Fig. 18 shows the velocity profile for nitrogen gas flow through the channel with hydraulic diameter of $D_h$ = 211 μm at a Reynolds number of 4696. The velocity profile illustrates that in the plenum chambers connected to the inlet and exit ports, the velocity is almost constant across the inlet port, flow accelerates due to sudden contraction and similarly across the exit port, a sudden deceleration is observed due to flow expansion. Within the channel, the velocity increases gradually in the initial region. Towards the exit of the channel, velocity increases rapidly due to gas acceleration resulting from the compressibility effects. The flow Mach number also follows a similar trend as the velocity. At the exit port, a maximum Mach number of 0.5 is observed, illustrating the need for accounting the compressibility effects. Both the static pressure and static temperature decrease at the inlet port and within the channel, as a result of flow acceleration. It is also evident that their variation becomes non-linear towards the exit of the channel. At the channel exit, a slight recovery of pressure and temperature is observed because of flow deceleration at the exit port.

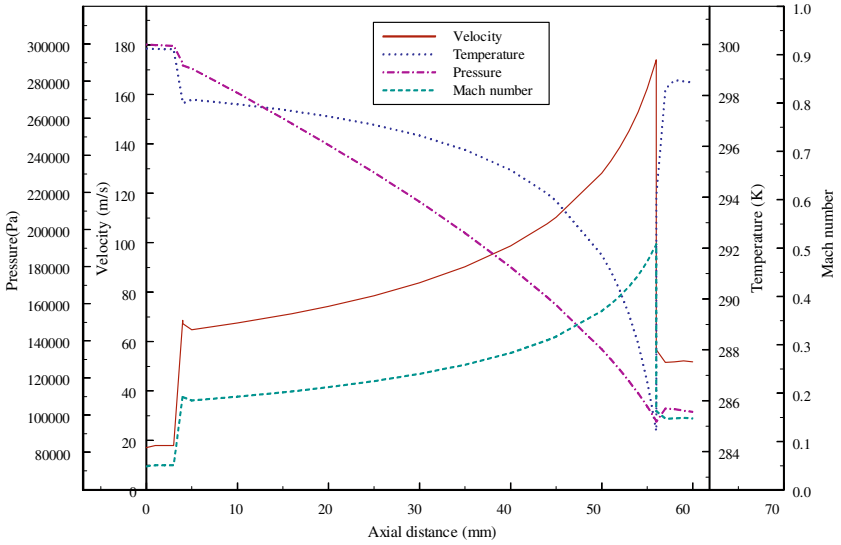


**Fig. 18.** Velocity, temperature, pressure and Mach number profiles for nitrogen flow through $D_h$ = 211 μm at Re = 4696.

Thus the present results of both, experimental and numerical investigations, clearly indicate the dominant role of compressibility for gas flow in the range of hydraulic diameters considered, which is distinct from the transition to turbulence. We did not observe any early transition as quoted by many earlier researchers. Neither did we observe delayed transition as observed by [8] at a Reynolds number as high as 6000. The observed transition Reynolds number of 1600–2300 is in near conformity with the conventional theory. Consistent with this observation, we found that numerical simulations based on the Navier–Stokes equations (with the inclusion of viscous dissipation) could predict the pressure profiles accurately in all regimes of flow.

## 6. Conclusions

By analyzing the axial pressure profiles obtained from the experiments as well as simulations with water and nitrogen gas as working fluids, it is possible to clearly differentiate the incompressible and compressible nature of flows in microchannels. As the developing length is substantial at higher Reynolds numbers in water flow, pressure loss due to flow development is to be considered along with the inlet and exit pressure losses, in calculating the friction factor. For gas flow through the channel, it is observed that when the exit Mach number approaches a value of 0.3, the flow is no longer incompressible, in conformity with existing theory and hence, incompressible correlations cannot hold good. At low Reynolds numbers and for exit Mach number below 0.3, both gas and water flow exhibit incompressible behaviour where the quantity $f$Re is constant within a value $\approx 53$, for the present shape of channels. For the gas flow $f$Re deviates from constant value even at low Reynolds numbers, due to the onset of compressible flow and not transition to turbulence. Hence, there is no early transition to turbulence as conjectured by Wu and Little [2]. As the channel diameter reduces, compressibility effects appear much earlier due to the flow acceleration resulting from large pressure drops, whereas the transition to turbulence is not affected much and occurs in the Reynolds number range of 1600 and 2300. The slight decrease in the transition range (usually it is from 2000 to 3500) may be due to the relative roughness or the edge effect of the trapezoidal channel geometry. We have not observed any delayed transition as claimed [8]. We also suggest that the deviation of $f$Re from a constant value is not an indicator of the onset of turbulence, but the deviation of slope of the $f$ vs Re curve and the curve becoming parallel to the Blasius solution are better indicators. The deviation from constancy of $f$Re in most of the cases is an indicator of the onset of compressible flow.

The axial pressure variation obtained through numerical simulation was compared with the experimental pressure profiles, for all the three microchannels. The results show that the simulated pressure profiles are in good agreement with the experimental values over the whole Reynolds number range, covering all the regimes of transition and compressibility. Hence, an axi-symmetric model can be used to analyze the pressure profile all along the length of the microchannel including port region. Also the conventional theory based on Navier–Stokes equations with viscous dissipation term and no-slip boundary conditions at the wall appear to be appropriate for the range of hydraulic diameters and Reynolds numbers considered.

## Acknowledgements

The authors acknowledge the help from Prof. Amitava Das Gupta and Prof. Nandita Das Gupta, Department of Electrical Engineering, IIT Madras, in the present work. They also acknowledge the financial support from Defence Research and Development Organisation (DRDO, India) and Department of Science and Technology (DST, India).

## References

[1] D.B. Tuckerman, R.F. Pease, High-performance heat sinking for VLSI, IEEE Electron Dev. Lett. 2 (1981) 126–129.
[2] P. Wu, W.A. Little, Measurement of friction factors for the flow of gases in very fine channels used for microminiature Joule–Thompson refrigerators, Cryogenics 23 (1983) 273–277.
[3] K.C. Pong, C.M. Ho, J. Liu, Y.C. Tai, Non-linear pressure distribution in uniform microchannels in application of microfabrication to fluid mechanics, ASME FED 196 (1994) 51–56.
[4] E.B. Arkilic, M. Schmidt, K. Breuer, Gaseous flow in long microchannels, J. Microelectromech. Syst. 6 (1997) 167–178.
[5] Z.X. Li, D.X. Du, Z.Y. Guo, Characteristics of frictional resistance for gas flow in microtubes, Proc. Symp. Energy Eng. 21st Century 2 (2000) 658–664.
[6] C. Chen, Numerical method for predicting three-dimensional steady compressible flow in long microchannels, J. Micromech. Microeng. 14 (2004) 1091–1100.
[7] S.E. Turner, L.C. Lam, M. Faghri, O.J. Gregory, Experimental investigation of gas flow in microchannels, J. Heat Transfer 126 (2004) 753–763.
[8] M.J. Kohl, S.I. Abdel-Khalik, S.M. Jeter, D.L. Sadowski, An experimental investigation of microchannel flow with internal pressure measurements, Int. J. Heat Mass Transfer 48 (2005) 1518–1533.
[9] X.N. Jiang, Z.Y. Zhou, X.Y. Huang, C.Y. Liu, Laminar flow through microchannels used for microscale cooling systems, IEE/CPMT Electronic Packaging Technology Conference, 1997.
[10] X.F. Peng, G.P. Peterson, B.X. Wang, Frictional flow characteristics of water flowing through rectangular microchannels, J. Exp. Heat Transfer 7 (1995) 249–264.
[11] N.T. Nguyen, D. Bochnia, R. Kiehnscherrf, W. Dözel, Investigation of forced convection in microfluid systems, Sensors Actuators A 55 (1996) 49–55.
[12] M. Richter, P. Woias, D. Weiß, Microchannels for applications in liquid dosing and flow-rate measurements, Sensors Actuators A 62 (1997) 480–483.
[13] D. Pfund, D. Rector, A. Shekarriz, A. Popescu, J. Welty, Pressure drop measurements in a microchannel, AIChE J. 46 (2000) 1496–1507.
[14] Z.X. Li, D.X. Du, Z.Y. Guo, Experimental study on flow characteristics of liquid in circular microtubes, in: Proceedings of International Conference on Heat Transfer and Transport Phenomena in Microscale, Begell House, New York, USA, 2000, pp. 162–168.
[15] H.Y. Wu, P. Cheng, Friction factors in smooth trapezoidal silicon microchannels with different aspect ratios, Int. J. Heat Mass Transfer 46 (2003) 2519–2525.
[16] P. Hao, H. Feng, K. Zhu, Flow characteristics in a trapezoidal silicon microchannel, J. Micromech. Microeng. 15 (2005) 1362–1368.
[17] M. Renksizbulut, H. Niazmand, Laminar flow and heat transfer in the entrance region of trapezoidal channels with constant wall temperature, J. Heat Transfer 128 (2006) 63–74.
[18] S. Colin, Rarefaction and compressibility effects on steady and transient gas flows in microchannels, Microfluidics Nanofluidics 1 (2005) 268–279.
[19] S.V. Garimella, C.B. Sobhan, Transport in microchannels – a critical review, Annu. Rev. Heat Transfer 13 (2003) 1–50.
[20] S.G. Kandlikar, W.J. Grande, Evolution of microchannel flow passages – thermo-hydraulic performance and fabrication technology, Heat Transfer Eng. 24 (2003) 3–17.
[21] F.M. White, Fluid Mechanics, fifth ed., McGraw-Hill Publication, New York, 2003.
[22] S.R. Turns, Thermal Fluid Science, first ed., Cambridge University Press, New York, 2006.